



Global back-arc extension due to trench-parallel mid-ocean ridge subduction

Yiming Liu^{a,b}, Lijun Liu^{b,*}, Yanchong Li^b, Diandian Peng^b, Zhiping Wu^a, Zebin Cao^b, Sanzhong Li^c, Qizhen Du^a

^a Shandong Provincial Key Laboratory of Deep Oil and Gas, School of geosciences, China University of Petroleum (East China), Qingdao, 266580, China

^b Department of Geology, University of Illinois at Urbana-Champaign, Urbana, 61801, USA

^c Frontiers Science Center for Deep Ocean Multispheres and Earth System, Key Lab of Submarine Geosciences and Prospecting Techniques, MOE and College of Marine Geosciences, Ocean University of China, Qingdao 266100, China



ARTICLE INFO

Article history:

Received 22 April 2022

Received in revised form 29 September 2022

Accepted 25 October 2022

Available online xxxx

Editor: A. Webb

Dataset link: <https://zenodo.org/record/3884294>

Dataset link: www.gplates.org/

Keywords:

mid-ocean ridge subduction
back-arc rifting
slab tearing
lithospheric stress
continental evolution

ABSTRACT

Subduction of young seafloors straddling mid-ocean ridges (MOR) is an inevitable consequence of plate tectonics. Surprisingly, this process correlates globally with prolonged back-arc extension when the MOR is largely trench-parallel. We investigate the underlying mechanism by analyzing the East China Sea Basin (ECSB) whose Cenozoic tectonic history consists of three syn-rift stages with the rift center progressively migrating oceanward. Global geodynamic models satisfying the past subduction history and present-day mantle structures successfully reproduce the lithospheric stress states of the evolving ECSB. We show that segmented removal of the Mesozoic Izanagi slab due to subduction of the young seafloor initiated Paleocene rifting within the western ECSB. Detachment of the former slab facilitated a strong landward mantle wind driven by the large pressure gradient across the slab. The resulting mantle traction pushed the thickened upper plate landward while entraining the young seafloors behind to slowly subduct, a process causing long-lasting Eocene extension of the central ECSB. The waning mantle wind after 30 Ma reduced basal traction and upper plate extension. A final phase of ECSB extension since the late Miocene formed the Okinawa Trough, when the subducting plate became old enough to trigger slab retreat. A similar dynamic scenario is also predicted in other circum-Pacific margins. We conclude that this enduring back-arc extension during MOR subduction represents an important mechanism for continental evolution during the closure of major ocean basins.

© 2022 Elsevier B.V. All rights reserved.

1. Introduction

Closure of major ocean basins on Earth consumed the underlying seafloors that inevitably led to subduction of mid-ocean ridges (MOR) below continents (Müller et al., 2016, 2019). A global analysis of continental deformation since Pangea separation repeatedly witnesses prolonged back-arc extension during the history of trench-parallel MOR subduction. These tectonic events occurred sequentially in South Asia (155–120 Ma), east Australia–north Antarctica (85–45 Ma), East Asia (65–23 Ma) and western U.S. (since 40 Ma), corresponding to the arrival and subsequent subduction of a MOR during the demise of the Tethys, Phoenix, Izanagi and Farallon oceanic plates, respectively (Müller et al., 2016, 2019) (Fig. 1). Although back-arc extension could be potentially attributed to a range of interacting causes, its intriguing correlation with the

trench-parallel MOR subduction suggests a previously unknown mechanism. This observation is puzzling because, according to the traditional wisdom, buoyant young seafloors resist subduction and should cause compression in the upper plate. Here we show that both the observed back-arc formation and associated MOR subduction reflects the long-lasting dynamic effect of mantle convergence during the terminal closure of a major oceanic plate.

The East China Sea Basin (ECSB, Fig. 2a) represents an ideal location for quantitatively understanding this surface-mantle interaction. First, the ECSB experienced strong Cenozoic tectonic deformation that is well preserved in the stratigraphy, in response to the Izanagi-Pacific MOR subduction (Fig. 2b). Second, the relatively mild amount of crustal extension (~150 km) within ECSB allows data-oriented geodynamic models (Peng et al., 2021a) to independently reproduce the underlying mantle processes without incorporating the basin extension as a boundary condition *a-priori*, thus avoiding potential circularity for inferring the surface-mantle relationship. Finally, a recent release of seismic data delineates

* Corresponding author.

E-mail address: ljliu@illinois.edu (L. Liu).

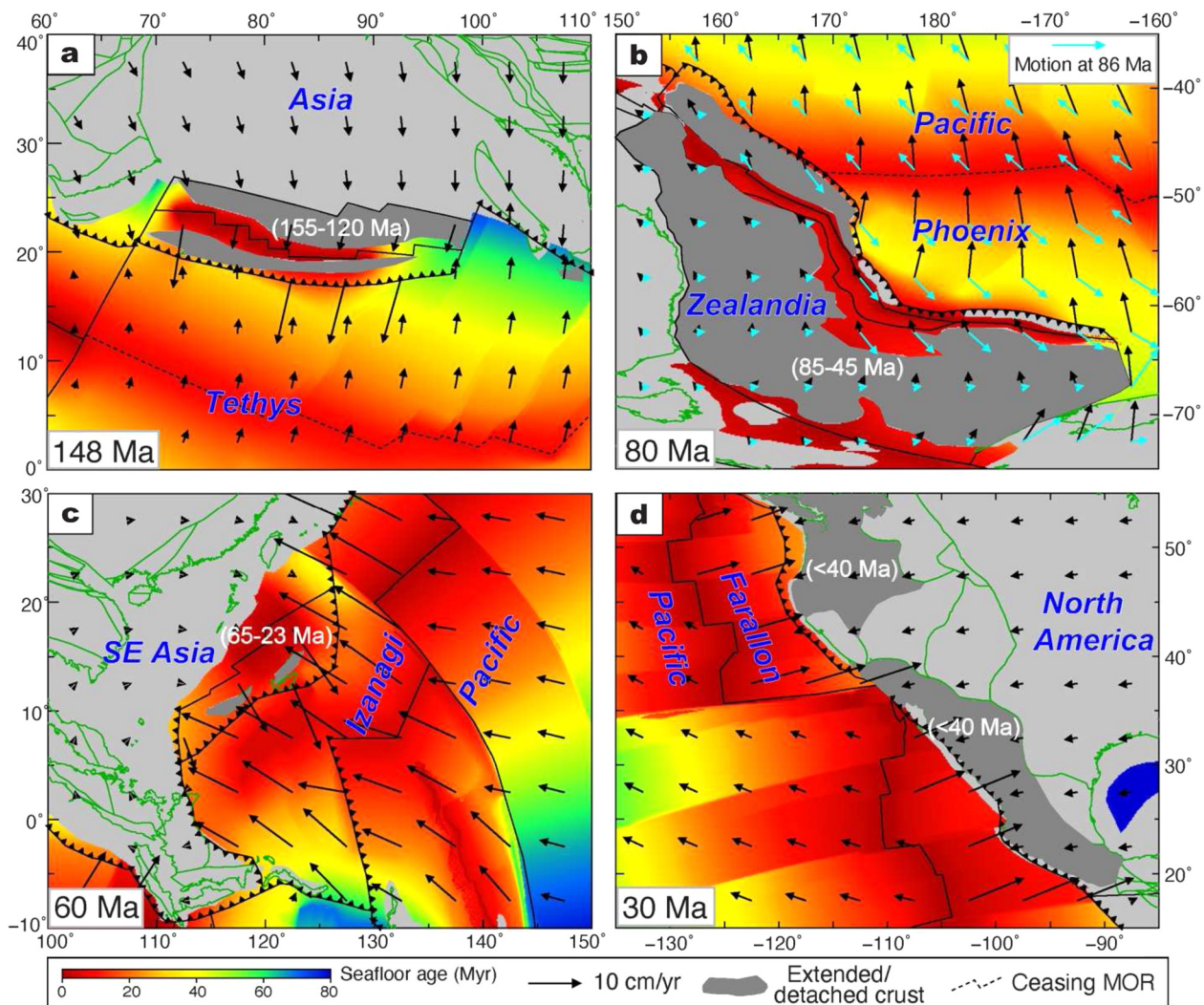


Fig. 1. Correlation of upper-plate extension with trench-parallel MOR subduction. a-d) Major extension events (duration marked in white and plate motion with arrows) corresponding to the subduction of four major MOR systems (Müller et al., 2016) that marked the closure of Tethys, Phoenix, Izanagi and Farallon oceanic basins since the Jurassic. (For interpretation of the colors in the figure(s), the reader is referred to the web version of this article.)

the ECSB kinematic history with unprecedented details, providing high-quality constraints on the underlying dynamics.

2. Methods

2.1. ECSB tectonic history

To investigate the tectonic configuration of the ECSB, we depicted the fault geometry and stratigraphic horizon based on the integration of the seismic data and well-logging data. Nine horizons (including T10, T12, T16, T20, T30, T40, T80, T100, Tg) and main controlling fault systems within the basin were recognized. To clarify the activity routines of the major faults in different periods, we calculated the dip-slip faulting rates of the NE-trending major faults following a reliable method (Huang et al., 2014). To reveal the tectono-sedimentary records, we produced structural maps for the syn-deposition fault distribution and isopach maps of the residual stratigraphic thickness, with the aid of the *GeoFrame* system provided by the Schlumberger company. To help further understand the coupled mantle-surface evolution as this study focuses on, we also collected the magmatic records during four different geological periods based on previous studies (Fig. 2a).

2.2. Global subduction models with data-assimilation

We reproduced past subduction since 200 Ma using a global-scale geodynamic simulation with data assimilation (Hu et al., 2018; Peng et al., 2021a). The initial thermal structure of oceanic plates (Fig. S1a) is derived from a modified plate model (Liu and Stegman, 2011). The evolving seafloor age that determines oceanic plate's thermal profile is based on a recent plate reconstruction (Müller et al., 2016). The continental plates have an initial steady-state geotherm (Fig. S1a), whose structure subsequently evolves in response to underlying mantle dynamics. The surface assimilates plate motions from the same plate reconstruction (Müller et al., 2016), whose assumption of rigid plate interiors with evolving plate boundary geometry helps avoid circular argument in predicting back-arc deformation. We assimilate data constraints only near the surface and away from convergent plate boundaries, such that slab morphology and associated mantle dynamics could evolve freely around subduction zones and inside the mantle.

The model considers realistic Earth structures, including crustal/mantle density due to both thermal and compositional effects, low-viscosity oceanic crusts near subduction zones, as well as various mineral phase transformations, all helping with the formation of more naturally looking asymmetric subduction and surface topography, relative to similar studies of this kind (Peng et al.,

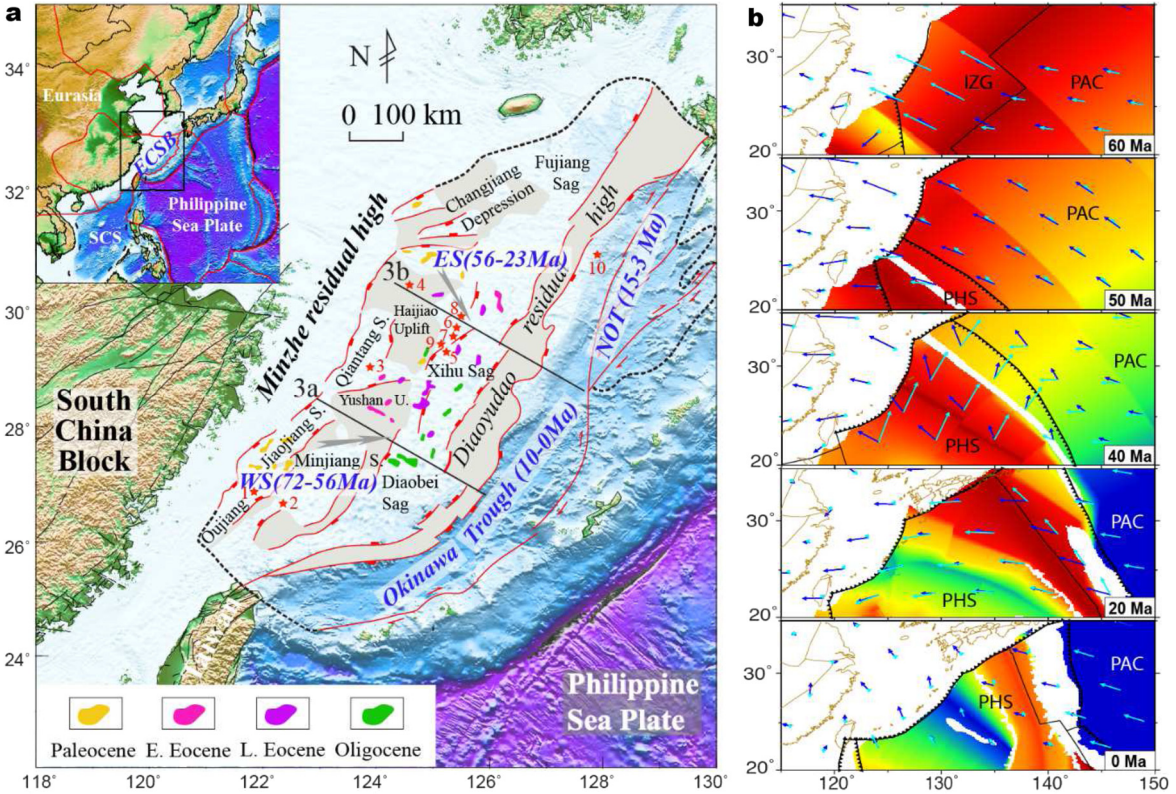


Fig. 2. Tectonic setting of the East China Sea basin (ECSB) and nearby subduction history. a) Distribution of sub-basins, volcanism, and their different formation ages. WS – West subbasins. ES – East subbasins. NOT – Northern Okinawa Trough. SCS – South China Sea. The red stars with numbers indicate well locations: 1 – SMT-1, 2 – FZ13-2, 3 – FY-1, 4 – HJ-1, 5 – TWT-1, 6 – PH-2, 7 – PH-3, 8 – PX-1, 9 – GS-1, 10 – TO-KA-1. b) Cenozoic history of seafloor age, plate motion (cyan arrows) and mantle flow (blue arrows, at 200 km depth) around ECSB including those during the Paleocene MOR subduction. IZG – Izanagi. PAC – Pacific. PHS – Philippine Sea.

2021b). This setup also helps the model to become dynamically compatible with the input surface kinematics soon after the initial condition.

We considered 13 different model compositions with a total number of about 1.8 billion chemical tracers. The continental lithosphere consists of a two-layer crust and three-layer mantle lithosphere. The average density of continental crust is about 2.8 g/cm^3 with the lower crust being weaker than the upper crust, to minimize the effect of imposed surface kinematics on lithospheric deformation at depth. The mantle lithosphere has a compositionally buoyant upper layer, a neutrally buoyant middle layer, and a dense lower layer, all relative to the ambient mantle (Hu et al., 2018). The oceanic plate has a surface layer, a basaltic crustal layer, and an underlying lithospheric mantle. The top layer is neutrally buoyant in composition and mainly mimics the viscosity effect of a weak and lubricating plate interface near the trenches upon subduction. Further below, we define a crustal layer whose density mimics that of the oceanic crust. When the chemically buoyant oceanic crust subducted to 120 km or deeper, its composition and density change following the basalt-to-eclogite phase transformation.

The viscosity structure is a function of temperature, composition, and depth. We adopt a four-layer background viscosity profile, where the values at 0–44 km, 44–410 km, 410–660 km, and 660–2,867 km are $10^{20} \text{ Pa}\cdot\text{s}$, $10^{20} \text{ Pa}\cdot\text{s}$, $10^{21} \text{ Pa}\cdot\text{s}$, and $3 \times 10^{22} \text{ Pa}\cdot\text{s}$, respectively (Fig. S1b). We also considered a viscosity increase at $\sim 1,000$ km depth from $3 \times 10^{22} \text{ Pa}\cdot\text{s}$ to $5 \times 10^{22} \text{ Pa}\cdot\text{s}$ according to some recent studies (Marquardt and Miyagi, 2015; Rudolph et al., 2015). Lateral viscosity variations come from both temperature and composition. Relevant to the evolution of slabs is a weak layer at the top of the oceanic plate, where a compositional multiplier is applied so that this layer has a minimum viscosity

of $10^{19} \text{ Pa}\cdot\text{s}$ near the trenches. Effectively, the models achieved up to four orders of lateral viscosity variation across the subduction zone. This is important for properly simulating the asymmetric subducting slabs, horizontal mantle flow and pressure, where the effective mantle and slab viscosities are inferred from matching present-day tomography and past geological records (Liu and Stegman, 2011, 2012; Hu et al., 2018; Peng et al., 2021a; Liu et al., 2021a).

The model results have been evaluated against independent data constraints in multiple recent studies. For example, the reproduced Cretaceous flat subduction below East Asia that is supported by the observed tectonic deformation and lithospheric structure in the region (Liu et al., 2021a; Peng et al., 2021a). The model predicted present-day mantle structure and slab geometry also closely match seismic tomography, with a key feature being the stagnant slabs below East Asia (Peng et al., 2021b). These studies provide additional independent supports on the modeled Cenozoic (between Cretaceous and present day) evolution of slabs and lithosphere relevant to this study (Figs. 4, 5).

2.3. Calculation of lithospheric stress

We use the depth-averaged model stress down to 90 km to represent the lithospheric stress state, following our recent work in quantifying North American crustal stress (Cao and Liu, 2021). In practice, we first integrate the horizontal components of the full 3D stress tensor over depth. Then, we obtain the depth-averaged horizontal full stress tensor to calculate the maximum compression orientations ($S_{H\max}$), which are shown as black bars in Fig. 5. The relative magnitudes of the three principal stresses within the lithosphere are represented through the $A\varphi$ parameter (Simpson, 1997; Cao and Liu, 2021). In practice, a value of $A\varphi$ smaller than 1

represents extension, that larger than 3 represents compression, and that in between represents transform.

3. Results and discussion

3.1. Tectonic history of the ECSB

The ECSB developed on the basement of the South China block (Fig. 2a) and represents an important component of the many marginal sea basins along East Asia (Suo et al., 2020) (Fig. 1c). The west Pacific margin experienced a complex tectonic history since the onset of Mesozoic subduction of the Izanagi Plate (Müller et al., 2016). Due to the sparsity of direct data constraints, the subduction history beneath the ECSB remains contentious (Müller et al., 2016; Wu et al., 2022). By compiling available well data (Fig. 2a, Table S1) and magma compositions (Yang et al., 2012; Zhao et al., 2016; Suo et al., 2019; Qi et al., 2021; Si et al., 2021), we show that there are widespread extrusive and intrusive magmas in the ECSB with ages ranging from the Early Cretaceous to the present (Table S1, Fig. 2a). The extrusive rocks mainly consist of andesite and intrusive rocks are mainly granite, whose major and trace element analyses all indicate an origin of island arc or continental arc since the Mesozoic (Yang et al., 2012; Zhao et al., 2016; Suo et al., 2019; Qi et al., 2021; Si et al., 2021). These results suggest that the ECSB region has experienced continuous subduction since the Cretaceous, as the recent plate reconstructions (Müller et al., 2016, 2019) properly describe. Consequently, the ECSB is a Meso-Cenozoic back-arc basin consisting of West subbasins, East subbasins and the Okinawa Trough, bounded by from west to east the Minzhe residue high, the Central uplift zone and the Ryukyu Islands (Lee et al., 2006; Zhu et al., 2019) (Fig. 2a). These subbasins further include multiple depressions distributed along the north-south direction that were separated by dominantly NEE-striking fault zones. Although previous studies have revealed the episodic jumps of extension centers within ECSB based on then-available seismic data (Liang and Wang, 2019; Zhu et al., 2019), the prototype basin in different stages remains obscure and a more quantitative analysis of the faulting and subsidence history is needed.

To map the detailed Cenozoic kinematic history of the ECSB, we utilize recently available high-resolution marine seismic and borehole data (see Method and Figs. 3 & S2 for more detailed information). These multi-channel seismic lines traverse the ECSB along the SW-NE orientation, with over sixty wells to calibrate horizon interpretation. We produced structural maps for the syn-deposition fault distribution and isopach maps of the residual stratigraphic thickness, with the aid of the *GeoFrame system* provided by the Schlumberger company. Overall, the age of syn-rift strata varies in space, outlining an eastward younging trend from the West subbasins to the Okinawa Trough.

The West subbasins are characterized by several independent grabens with an asymmetric pattern, where Paleocene-dominant strata are bounded by unconformity horizons Tg (72 Ma; see Fig. S2 for time scale) at the base and T80 (56 Ma) on top of the syn-rift deposition (Fig. 3a; Fig. S2). The East subbasins host thick Eocene strata (E_{20+w} and E_{2p}) where the syn-rift sequence was bounded by horizon T20 (23 Ma) at the top and horizon T80 (56 Ma) at the base. The main rifting structures were developed under T30 (~32 Ma), marking the stage of strongest extension. The simultaneous occurrence of many minor faults within the strata further indicates enhanced rifting during this period. The presence of intensive flexural deformation within the subsequent Oligocene and Miocene strata (between horizons T30 and T12) reveals the imprint of post-23 Ma transpressional deformation over the region (Fig. 3a-c).

The Okinawa Trough formed as a NE-NNE orientated graben with basement metamorphic rocks overlain by Late Neogene and

Quaternary syn-rift strata. Two distinctive features are observed: a) Rifting initiated in the northern Trough at ~15 Ma and jumped to the middle and southern segment of the Trough after 3 Ma (Fig. 2a). b) Numerous nearly vertical normal faults developed in the southern part with the formation of sliding terrace structure (Fig. 3a-c), demonstrating intensive shearing deformation alongside rapid EW extension, consistent with the southward propagating deformation within the easternmost ECSB (Fig. 2a).

The spatial-temporal migration of ECSB deformation is further reflected in the evolution of depocenters. Paleocene sediments predominantly deposited within West subbasins in the Qiantang, Oujiang and Minjiang sags, with the maximum thickness exceeding 2600 m; a minor amount occurred in the isolated Changjiang Depression on the north (Figs. 2a, 3c). Eocene deposition concentrated mostly within the East subbasins (>4000 m in thickness), with a lesser amount further west (Fig. 3c). Intensive syn-rifting deposition restarted during the late Miocene, but mostly in the Okinawa Trough (Liu et al., 2016; Wei et al., 2021), where the lack of sediments in the south Trough is likely due to both inadequate data coverage and the recent (post-3 Ma) onset of subsidence. A similar migration pattern is observed in the vertical intensity of main controlling faults (Fig. 3d). The peak dip-slip faulting rates in West subbasins (No. 1 and No. 2 fault zone) reached the pinnacle during the Paleocene when the maximum rate temporally exceeds 400 m/Myr. The main controlling faults of East subbasins (No. 3 and No. 4 fault zone) experienced intensive faulting during the Eocene with the maximum rate around 300 m/Ma. Further east, intensive normal faulting in the Okinawa Trough initiated in the latest Miocene and lasted till the Quaternary. A detailed tectono-sedimentary evolution history of the ECSB is further illustrated in the balanced cross-section analysis (Fig. 4).

3.2. Subduction dynamics and lithospheric deformation below ECSB

To reproduce the past subduction and lithospheric deformation beneath East Asia, we performed four-dimensional geodynamic models that satisfy the past plate motion, seafloor age and plate geometry (Hu et al., 2018) (see Method for more details). We utilized a recent plate reconstruction (Müller et al., 2016) that does not incorporate deformable continental margins, such that the resulting mantle dynamics is not forced by the known basin kinematics. These subduction models have been shown to match the present mantle structures (Peng et al., 2021a) and Mesozoic tectonic constraints (Liu et al., 2021a; Peng et al., 2021b) within East Asia. A comparison of the best-fit model with three seismic tomography images along two E-W cross sections in North China and South China (Fig. S3) reveals that both the position and geometry of reproduced slabs well match those observed throughout the mantle.

Here we further analyze the simulated subduction history below the ECSB. Of direct relevance to the Cenozoic ECSB evolution is the formation of the East Asian stagnant slabs. In a recent study (Peng et al., 2021a), we showed that the stagnant slabs beneath South China consist of the subducted Philippine Sea (PHS) slab on the west and Pacific (PAC) slab to the east (Fig. S3a). In a map view, the modeled stagnant slab below South China (Fig. 5a) also resembles that observed (Fig. S4). Here we further illustrate this slab feature along a trench-normal profile through the central ECSB (Fig. 5). The modeled slab geometry (Fig. 5b) displays a good match with that from the three tomography images (Fig. 5c-e). The time evolution of these slabs more intuitively demonstrates that the western stagnant piece represents the PHS slab subducted since 50 Ma (Fig. S5), a conclusion that differs from most other studies. This finding corroborates the above inference based on magmatic records that the ECSB has been in the back-arc location since the Mesozoic.

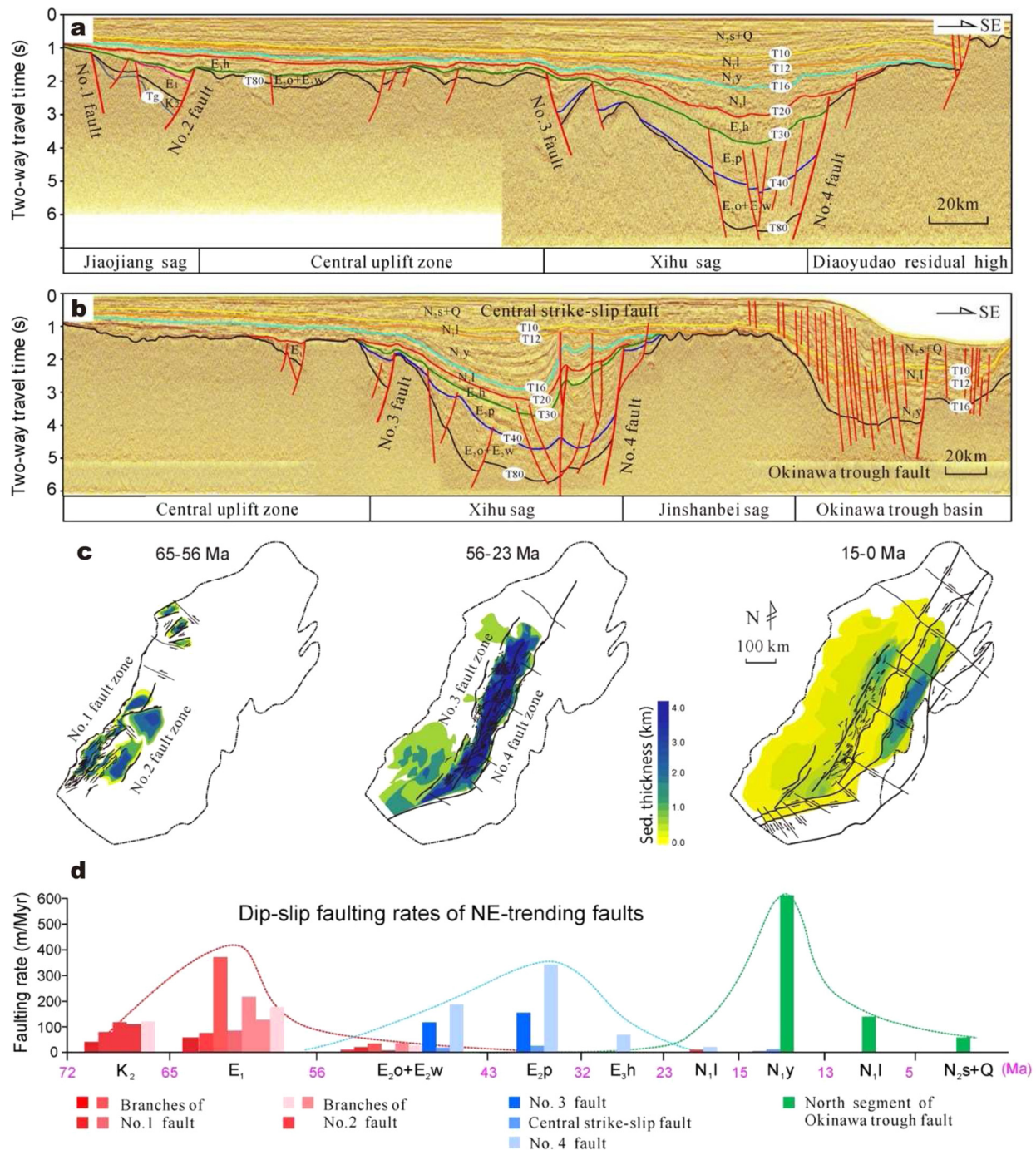


Fig. 3. Cenozoic rifting history of the ECSB. a-b) Typical seismic cross sections across the northern and southern parts of the ECSB, with horizon and formation names listed in Fig. S2. c) Isopach maps showing the residual stratigraphic thickness of the ECSB. d) Dip-slip faulting rates of syn-depositional faults in different stages. The red columns indicate faulting rates in West subbasins, blue for East subbasins, and green for Okinawa Trough.

Following the ECSB extension history, we examine the model evolution and lithospheric stress since 70 Ma (Figs. 6, 7). To make sure that the imposed surface kinematics in the sequential data-assimilation simulation is dynamically compatible with the simulated mantle processes, we recalculated all geodynamic properties at each time snapshot by setting the surface to freely slip while keeping the buoyancy and viscosity structures of the model unchanged. The resulting subduction and mantle velocities for all times (Fig. S6) are nearly identical to those in the reference cases (Fig. 6). We further compared the key forces of the two models: dynamic topography that drives flow, and output mantle stresses (Fig. S7). Both lithospheric pressure and stress differ, as reflect

their different surface boundary conditions: the case with imposed plate kinematics diminishes intraplate deformation and stresses, while the case with a free-slip surface has clear internal deformation, especially within continents. Importantly, below the lithosphere, the convective mantle has all three quantities (mantle flow, dynamic pressure, and mantle and slab stresses) that are nearly identical, suggesting that the mantle dynamics is indeed compatible with the observed surface kinematics. The presented lithospheric stress results (averaged within the upper 90 km depth; Fig. 7) are based on these fully dynamic calculations.

Prior to the onset (~ 70 Ma) of ECSB extension, the gradual buildup of pressure gradient across the slab hinge (Fig. S8a)

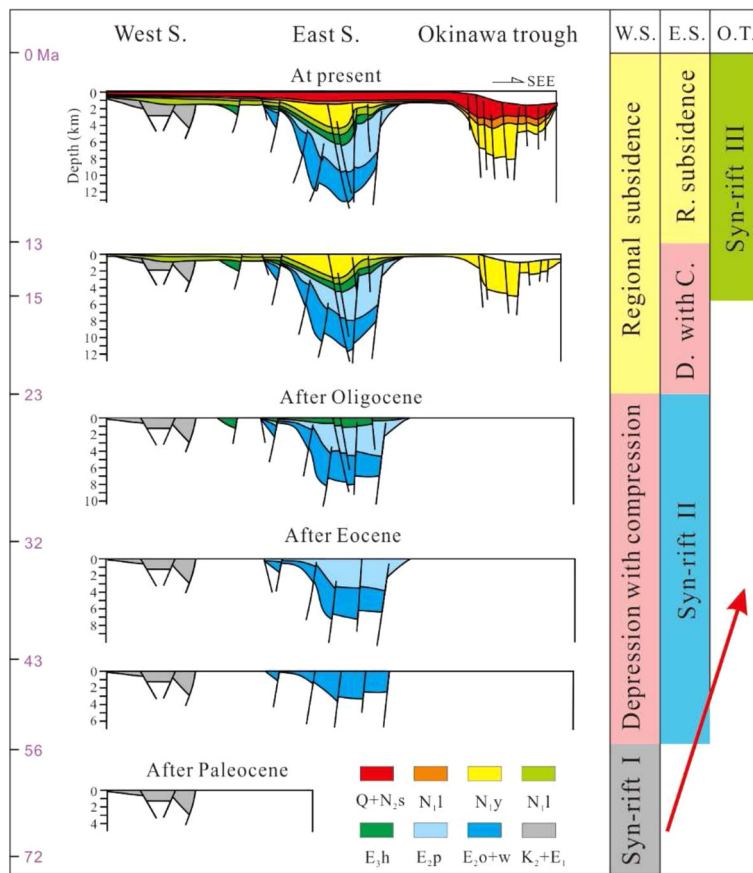


Fig. 4. Three episodic rifting history of the ECSB revealed by the balanced cross-section analyses. The West subbasins initiated the rifting during 72–56 Ma. The rifting center migrated to the East subbasins rifted during 56–23 Ma, and the Okinawa trough suffered intensive rifting from 15 Ma until present.

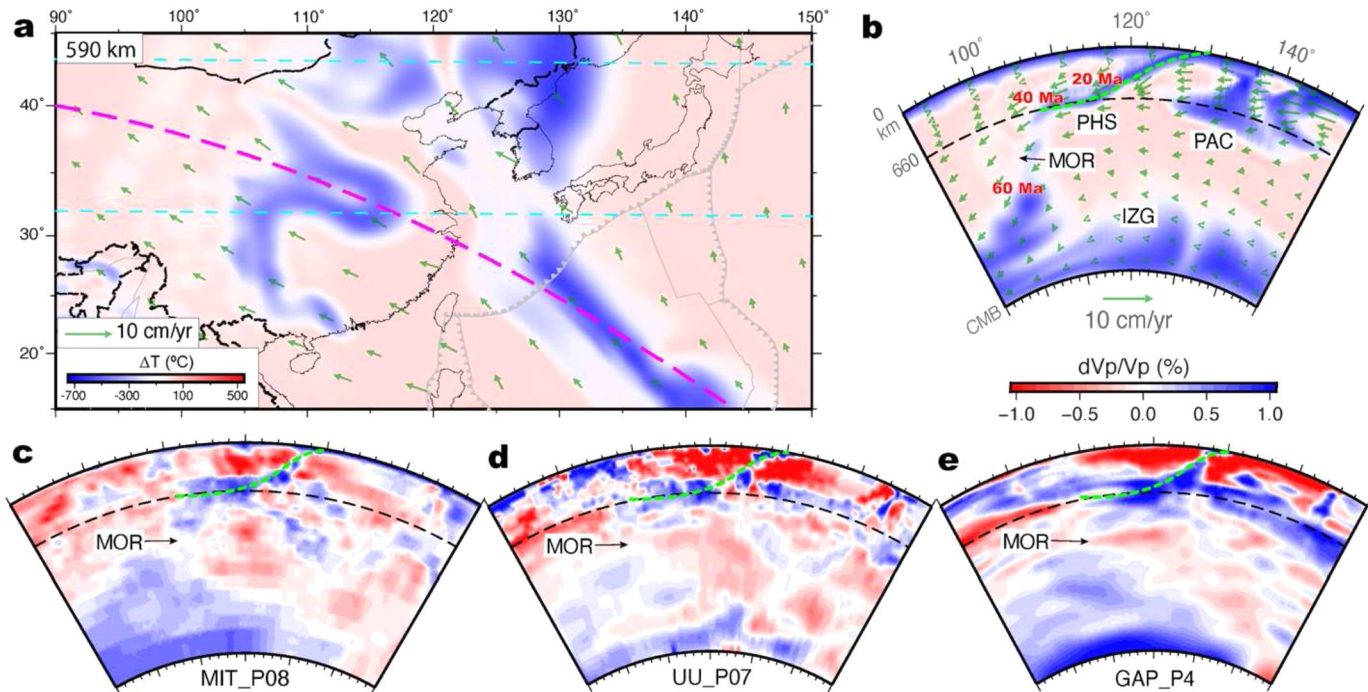


Fig. 5. Modeled vs. observed PHS slab beneath South China. (a) Map view of the simulated present day mantle thermal structure at 590 km. Cyan dashed lines mark locations of cross sections in Figure S3. (b) Cross-sectional view of the modeled PHS slab (green dashed line) along the profile shown as the magenta curved dashed line in a. The initial subduction age of each segment of the PHS-IZG slabs is annotated in red. IZG – Izanagi. PAC – Pacific. PHS – Philippine Sea. (c-e) Mantle structure along the same cross section in three different P-wave tomography images, MIT_P08 (Li et al., 2008), UU_P07 (Amaru, 2007), and GAP_P4 (Obayashi et al., 2013).

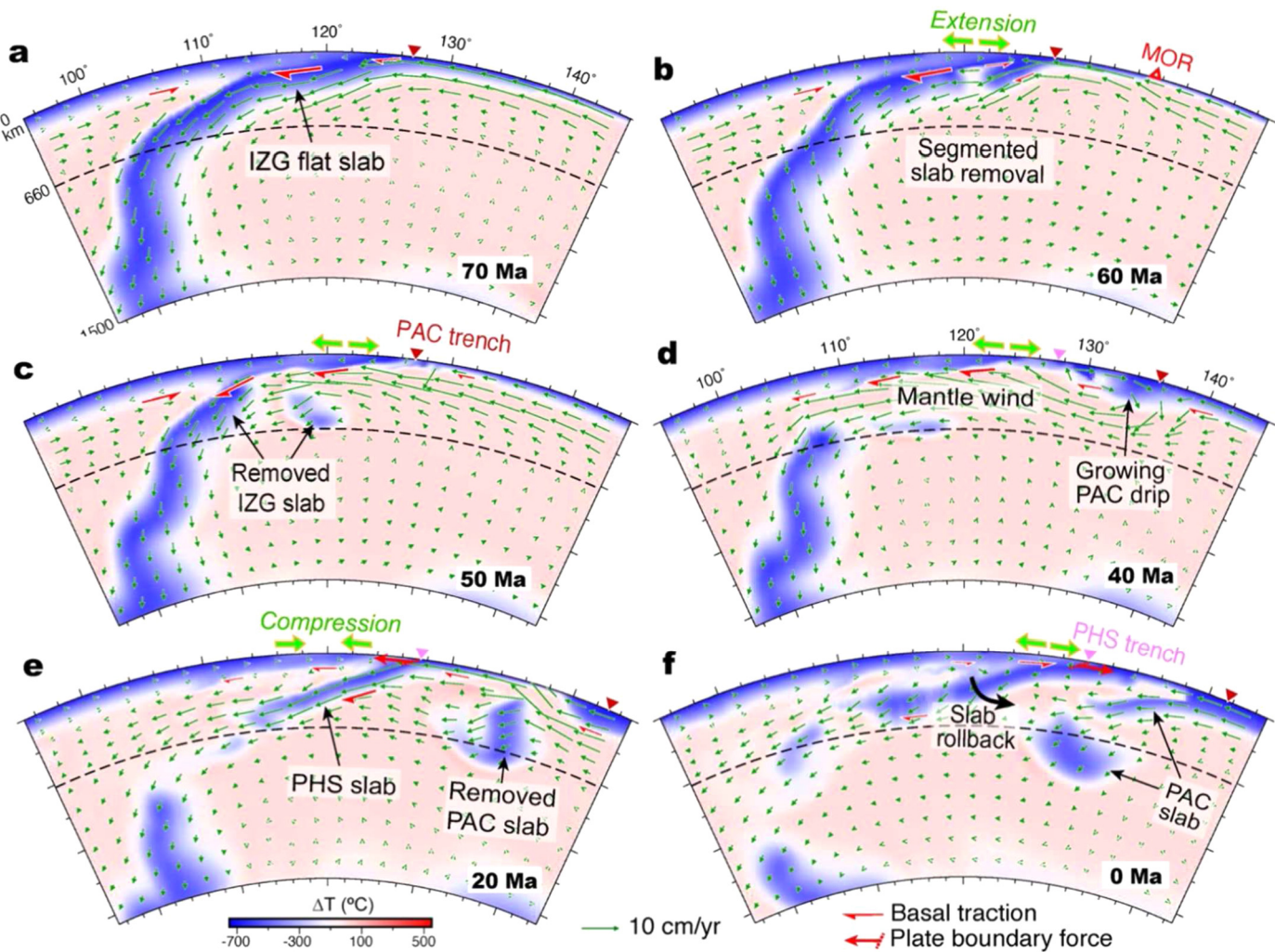


Fig. 6. Evolution of subduction and mantle flow along 30°N since 70 Ma. The background color represents temperature anomaly relative to the ambient mantle. Thin green arrows denote mantle flow. Bold green arrows at the surface indicate the deformation style of the continental margin.

formed a broad flat slab beneath South China by the Late Cretaceous (Peng et al., 2021b) (Fig. 6a), corresponding to the observed widespread basin inversion, orogenic uplift and lithospheric thinning above the flat slab (Liu et al., 2021a). During the latest Cretaceous to earliest Cenozoic, the rapidly decreasing age of the Izanagi seafloor (Fig. 2b) caused the slab to thin and weaken (Fig. 6a) that ultimately led to a fragmentation in the tail of the flat slab (Fig. 6b). The continuous landward translation of the older slab that thickened the continental root where this slab eventually steeped and foundered (Fig. 6c) and the delamination-style removal of the younger slab created an asthenospheric pathway between them (Fig. 6b-c) that allowed upwelling to occur, consistent with the observed Paleocene volcanism within the West subbasins of the ECSB (Fig. 2a). Examination of the ECSB lithospheric stress (maximum compression direction and the $A\varphi$ parameter, refer to Method for description) reveals a distinct transition from prominent compression at 80 Ma (Fig. S9a) to transtension at 70 Ma and then to prominent extension at 60 Ma (Fig. 7a-b). This stress state transition is due to the segmented removal of the former flat slab that gradually relaxed previous upper-plate compression (Fig. 6a-c). The thickened lithospheric root landward of the back-arc region blocked the lateral mantle flow, as can be seen from the abrupt decrease of flow velocity toward the root. This resulted in a landward viscous push (via both pressure drag and viscous drag) exerted on the South China block, which further enhanced extension in the back-arc on the ocean side, a process that maintained through-

out the early Cenozoic (Fig. 7b-d). Spatially, the predicted pattern of Paleocene ECSB extension also correlates strongly with the observed rifting within the West subbasins (Figs. 2a, 3c).

Segmented removal of the former Izanagi slab with the approach of the MOR during the Paleocene (Fig. 6b-c) exposed the depressurized mantle wedge to the over-pressurized oceanic mantle on the east (Fig. S8a-c), exciting a strong landward mantle flow that lasts till the present day, and we defined this flow feature as a mantle wind (Peng et al., 2021a) (Figs. 2b, 6, S8d-h). Analyses of plate motion, slab evolution, and lithosphere stress, as detailed below, suggest that this strong landward mantle wind has largely controlled the Cenozoic geodynamics of the East Asian margin.

An important question raised at the beginning of this work is: what caused the many young seafloors including MORs to subduct during the closure of major oceans (e.g., Fig. 1)? We find that the landward mantle wind formed after the fragmentation of the former slab is a key driver. This is shown as the continuous trenchward motion, albeit at reduced rates, of the young Izanagi, Pacific and Philippine Sea plates after 60 Ma, both observed (Figs. 2b, 6) and predicted (Fig. S6). This could also be seen from the stress states within the outer rise region of the oceanic plates: the continuous Izanagi slab pull generated extension within the incoming oceanic plates prior to 60 Ma (Figs. 7a-b, S9a), while this switched to strong compression after the slab removal (Figs. 6c-e, S9b), indicating the resistance of young seafloors to subduction that was forced by the underlying mantle entrainment. The slow growth of

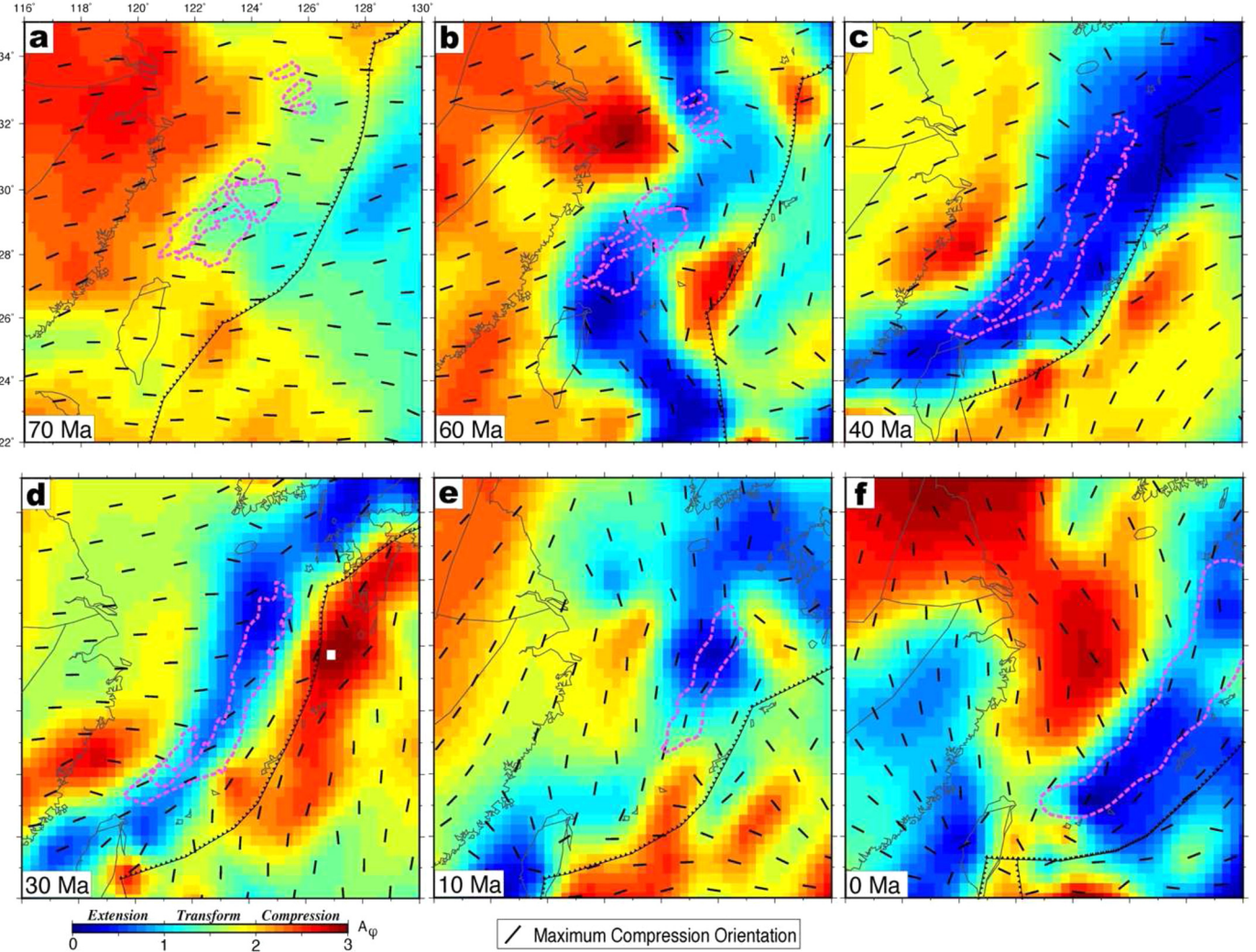


Fig. 7. Calculated lithospheric stress states during major Cenozoic basin formation events. Black bars represent the horizontal maximum compression orientation and the background color represents the A_φ parameter. Magenta outlines mark the extent of ECSB subsidence, where that over 70–10 Ma is based on the sedimentation history in Fig. 3c, and that at 0 Ma is based on topography in Fig. 2a. The present-day coastlines are rotated backward for location purposes.

a drip-shaped cold material below the Pacific trench (Fig. 6d) and its eventual delamination (Fig. 6e) further reflects the nature of this forced subduction.

Besides forcing the Izanagi-Pacific MOR system and the young Philippine Sea plate to subduct, the strong mantle wind also pushed the overriding continental lithosphere on the west landward (e.g., Fig. 6c-d). This is further illustrated as compressional stress west of the ECSB (Fig. 7b-d). Consequently, a broad back-arc region in between them experienced long-lasting stretching due to the tendency of the South China block to move away from the trench where subduction was temporarily choked. The computed Eocene-Oligocene ECSB extension (Fig. 7c-d) closely matches that of observed basin kinematics (Figs. 2a, 3c), where the rifting region, indicated by both the maximum compression orientation and the spatial distribution of A_φ , is strictly trench-parallel and east of the Paleocene basins. The associated shallow mantle upwelling below this region (e.g., Fig. 6d) further explains the abundant volcanism within the East subbasins (Fig. 2a).

According to the adopted plate reconstruction, the Philippine Sea plate occupied the trench east of the ECSB after 50 Ma (Fig. 2b), and the Pacific plate subducted beneath the Philippine Sea plate further east. Our calculations suggest that the Philippine Sea plate subduction had likely been passive until the late Miocene. For example, the stress within the outer rise region had

been compressional during 40–10 Ma (Fig. 7c-e), and the landward mantle flow had been leading the motion of the Philippine Sea slab (Figs. 5d-f, S6). During this period, the westward mantle wind gradually descended to the base of the upper mantle, following the sinking Izanagi slab that produced the low pressure below the continent (Peng et al., 2021a) (thus the origin of the mantle wind). Consequently, the basal traction on the thick South China lithosphere diminished over time, and the mantle flow was consumed by forcing the young seafloors to subduct, as is expressed as the diminishing ECSB extension since 40 Ma (Fig. 7c-d). Upper plate extension terminated by ~23 Ma (Fig. 2a), consistent with the westward mantle wind blocked by the Philippine Sea slab at 20 Ma (Fig. 6e) and the deepened lateral pressure gradient (Fig. S8e-f) mainly to drive slab advance (Fig. 6e).

As the mantle wind descent further toward the present day, its effect on forcing Philippine Sea subduction eventually diminished (Figs. 6f, S8). Consequently, the increasing age, thus negative buoyancy, of the Philippine Sea slab (Fig. 2b) started to control its own subduction and the slab started to roll back (Fig. 6e-f). This transition reinitiated ECSB extension in the late Miocene, starting at the northern Okinawa Trough (Fig. 7e) where the seafloor is older (Fig. 2b) and subsequently along the entire Trough toward the present (Fig. 7f), both closely mimicking observation (Figs. 2a, 4c-d).

3.3. Implications on mechanisms of back-arc evolution and MOR subduction

The fundamental dynamics of the Cenozoic rifting history of the ECSB is the long-lasting converging mantle (Peng et al., 2021a) (Figs. S6, S8) whose surface expression was modulated and partitioned by the subduction of young seafloors around the Izanagi-Pacific MOR: 1) prior to the arrival of the MOR, the well-established mantle convergence due to the lateral pressure gradient (Fig. S8a) below the continental margin formed a flat Izanagi slab (Peng et al., 2021b); 2) subduction of the young Izanagi seafloor during latest Cretaceous to earliest Cenozoic caused the flat slab to be stretched apart by the pressure gradient, where the resulting differential basal shear initiated Cenozoic extension along the margin; 3) the fragmented detachment of the slab excited a fast landward mantle wind driven by the lateral pressure gradient (Fig. S8b-e), where the resulting basal traction, combined with retarded subduction along the trench, caused the upper plate to extend widely; 4) the enduring basal traction also forced the young seafloors to subduct (Fig. 6d-e), a process that became self-sustaining only when the incoming oceanic plate grew old enough during the late Cenozoic (Fig. 6f).

Our predicted slab detachment prior to MOR subduction is due to the competition between slab buoyancy and weakening (Gurnis et al., 2004). The strong landward mantle flow during slab break off is commonly observed in both generic models (Burkett and Billen, 2009; Shen and Leng, 2021) and those simulating the circum-Pacific subduction history (Peng et al., 2021a; Liu and Stegman, 2012; Zhou et al., 2018a, 2018b). However, the transition of upper-plate compression to extension during slab detachment in our calculation contrasts with models assuming an initially normal slab dip that generates dominant extension (e.g., Burkett and Billen, 2009). This is related to the flat Izanagi slab prior to MOR subduction supported by East Asian geology and lithospheric evolution (Peng et al., 2021b; Liu et al., 2021a), and the subsequent landward mantle flow that was blocked further inland by its thick root (Fig. 6), similar to that occurred in the western U.S. since the mid-Miocene (Zhou et al., 2018a, 2018b). Here we consider the stress instead of strain of the upper plate because the former better reflects the buoyancy effect of the underlying convective mantle that is effectively achievable by reproducing the subduction history through data-assimilation modes (Peng et al., 2021a, 2021b), while the latter further requires an accurate representation of the highly non-linear rheology of the continental lithosphere (Liu and Hasterok, 2016; Liu et al., 2021b; Chen et al., 2020; Gerya et al., 2021) that is difficult to achieve in reality, especially for global-scale models.

There are multiple alternative proposed mechanisms for back-arc extension, including landward movement of the overriding plate (Lallemand et al., 2005), initial subduction causing trench retreat (Faccenna et al., 2017), and toroidal flow around slab edges (Schellart et al., 2007). Recent plate reconstructions suggest that during the major tectonic events associated with MOR-subduction, the overriding plates were either moving toward the trench (Fig. 1a, d) or largely stationary (Fig. 1b, c). In addition, all these extension events occurred long (>50 Myr) after subduction initiated and were mostly above the interior of wide slabs (Müller et al., 2016) (Fig. 1). Therefore, we conclude that these previous hypotheses cannot explain the observed back-arc deformation associated with the Tethyan and Panthalassan MOR subduction (Fig. 1).

On the other hand, the strong similarity of the tectonic setting (MOR subduction) and duration (~40 Myr) of ECSB to those in Fig. 1 suggests that these tectonic events were likely governed by the same geodynamic mechanism. Without repeating all the analyses done for ECSB, we present some snapshots of the calculated lithospheric stress for these locations based on the same geody-

namic simulation. Due to the early age of the two Mesozoic events (Fig. 1a-b), we only adopted the model results during the Cretaceous time, to avoid potential effect of the uncertain model initial condition. For the two Cenozoic events (Fig. 1c-d), we present the results both before and after the onset of extension. We can clearly see that the computed lithospheric stress evolution closely resembles the observed tectonic history for all four locations (Fig. 8). This confirmed relationship of back-arc extension with young seafloor subduction further supports our proposed mechanism of differential basal traction associated with lateral mantle flow during fragmented slab removal (Fig. 6). We realize the larger uncertainties in the earlier events, so more emphasis should be laid on the younger ones. For example, our new mechanism well explains the coeval onset of Cenozoic Basin & Range extension within the western U.S. (McQuarrie and Wernicke, 2005), reestablishment of the Cascadia arc (Dickinson, 2006; Liu et al., 2021b), and resumed high-angle Farallon subduction at ~40 Ma (Liu and Stegman, 2011) corresponding to a major gap in the mantle seismic image (Schmandt and Lin, 2014).

4. Conclusions

By dynamically linking the subduction history of young seafloors with the evolving stress state of continental convergent margins, we identified a new mechanism for the widespread formation of back-arc basins. We show that the landward mantle wind after the detachment of a former flat slab caused the continental margin to extend when this flow encounters and pushes the thick continental roots behind the basin, a long-lasting process controlled by the sinking of the former slab.

In addition, this study also provides important new insights on the driving mechanism of young seafloor subduction during the closure of major oceans. The enduring westward mantle wind below East Asia that had promoted continuous subduction of the Paleocene MOR and associated young seafloors echoes the recent proposals for the need of basal traction to explain the late Cenozoic Pacific motion (Stotz et al., 2018) and formation of the East Asian stagnant slabs (Peng et al., 2021a). Similarly, an eastward mantle flow has been recently proposed to explain the migratory Yellowstone volcanism (Zhou et al., 2018a) and the peculiar seismic anisotropy pattern within the western U.S. (Zhou et al., 2018b). Collectively, the strong landward basal traction due to mantle flow originated from slab detachment could act as a key force for the subduction of young seafloors. This could manifest as either continued MOR subduction along the same trench or ridge captured by the neighboring plate. In both cases, the young seafloors would be eventually subducted, paving the way toward the ultimate closure of the paleo ocean.

Code availability

The mantle convection code CitcomS is available at www.geodynamics.org/cig/software/citcoms/. The GMT software package used to make figures can be downloaded at www.soest.hawaii.edu/gmt/.

CRediT authorship contribution statement

Yiming Liu: Conceptualization, Investigation, Writing – original draft. **Lijun Liu:** Conceptualization, Methodology, Supervision, Writing – review & editing. **Yanchong Li:** Data curation, Visualization. **Diandian Peng:** Methodology, Software. **Zhiping Wu:** Resources, Supervision, Validation. **Zebin Cao:** Methodology, Visualization. **Sanzhong Li:** Validation, Writing – review & editing. **Qizhen Du:** Investigation, Validation.

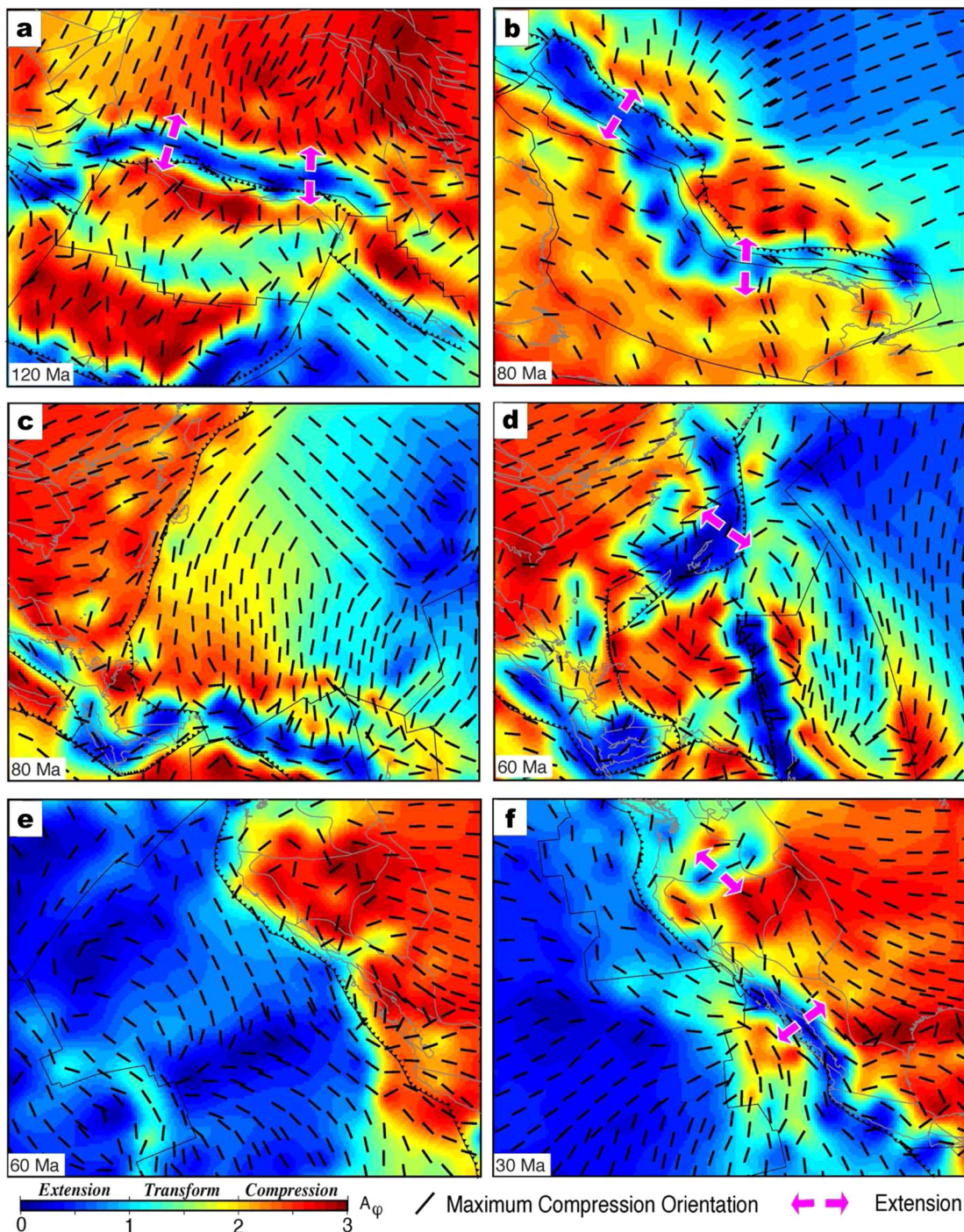


Fig. 8. Computed lithospheric stress during the four observed tectonic events associated with subduction of major MORs (Fig. 1). These locations include a) South Asia, b) east Australia-north Antarctica, c, d) East Asia, and e, f) western United States.

Declaration of competing interest

The authors declare that they have no known competing financial interests or personal relationships that could have appeared to influence the work reported in this paper.

Data availability

All materials of this study are available upon request from the corresponding author.

The geodynamic model output of slab geometry, temperature field, and mantle flow are available at <https://zenodo.org/record/3884294>.

The plate reconstruction models (Müller et al., 2016, 2019) and the GPlates software tool used in this study are available at: www.gplates.org/.

Acknowledgement

This work has been financially supported by the Laboratory for Marine Mineral Resources, Qingdao National Laboratory for Ma-

rine Science and Technology (2021QNLMO20001-1), China Postdoctoral Science Foundation (2022M713461), National Natural Science Foundation of China (42072169, 41930429), National Science Foundation of the U.S.A. (EAR1554554), and the Fundamental Research Funds for the Central Universities (22CX06005A). We gratefully acknowledge the Research Institute of the CNOOC (China National Offshore Oil Corporation) for providing seismic data and well data for this work. We thank the Editor-in-chief, Prof. Alexander Webb, Prof. Taras Gerya at ETH Zurich and an anonymous reviewer for their significant comments and suggestions, which substantially improved the manuscript.

Appendix A. Supplementary material

Supplementary material related to this article can be found online at <https://doi.org/10.1016/j.epsl.2022.117889>.

References

- Amaru, M.L., 2007. Global Travel Time Tomography with 3-D Reference Models. Utrecht University.
- Burkett, E.R., Billen, M.I., 2009. Dynamics and implications of slab detachment due to ridge–trench collision. *J. Geophys. Res., Solid Earth* 114, B12402.
- Cao, Z., Liu, L., 2021. Origin of three-dimensional crustal stress over the conterminous United States. *J. Geophys. Res., Solid Earth* 126, e2021JB022137.
- Chen, L., Liu, L., Capitanio, F., Gerya, T., Li, Y., 2020. The role of pre-existing weak zones in the formation of the Himalaya and Tibetan Plateau: 3-D thermomechanical modelling. *Geophys. J. Int.* 221, 1971–1983.
- Dickinson, W., 2006. Geotectonic evolution of the Great Basin. *Geosphere* 2, 353–368.
- Faccenna, C., Oncken, O., Holt, A.F., Becker, T.W., 2017. Initiation of the Andean orogeny by lower mantle subduction. *Earth Planet. Sci. Lett.* 463, 189–201.
- Gerya, T.V., Bercovici, D., Becker, T.W., 2021. Dynamic slab segmentation due to brittle–ductile damage in the outer rise. *Nature* 599, 245–250.
- Gurnis, M., Hall, C., Lavier, L., 2004. Evolving force balance during incipient subduction: evolving force balance. *Geochem. Geophys. Geosyst.* 5, GC000681.
- Hu, J., Liu, L., Zhou, Q., 2018. Reproducing past subduction and mantle flow using high-resolution global convection models. *Earth Planet. Phys.* 2, 189–207.
- Huang, L., Liu, C., Wang, Y., Zhao, J., Mountney, N.P., 2014. Neogene–Quaternary postrift tectonic reactivation of the Bohai Bay Basin, eastern China. *AAPG Bull.* 98, 1377–1400.
- Lallemand, S., Heuret, A., Boutelier, D., 2005. On the relationships between slab dip, back-arc stress, upper plate absolute motion, and crustal nature in subduction zones. *Geochem. Geophys. Geosyst.* 6, Q09006.
- Lee, G.H., Kim, B., Shin, K.S., Sunwoo, D., 2006. Geologic evolution and aspects of the petroleum geology of the northern East China Sea shelf basin. *AAPG Bull.* 90, 237–260.
- Li, C., van der Hilst, R.D., Meltzer, A.S., Engdahl, E.R., 2008. Subduction of the Indian lithosphere beneath the Tibetan Plateau and Burma. *Earth Planet. Sci. Lett.* 274, 157–168.
- Liang, J., Wang, H., 2019. Cenozoic tectonic evolution of the East China Sea Shelf Basin and its coupling relationships with the Pacific Plate subduction. *J. Asian Earth Sci.* 171, 376–387.
- Liu, L., Hasterok, D., 2016. High-resolution lithosphere viscosity and dynamics revealed by magnetotelluric imaging. *Science* 353, 1515–1519.
- Liu, B., Li, S., Suo, Y., Li, G., Dai, L., Somerville, I.D., Guo, L., Zhao, S., Yu, S., 2016. The geological nature geodynamics of the Okinawa Trough, Western Pacific. *Geol. J.* 51, 416–428.
- Liu, L., Liu, L., Xu, Y., 2021b. Mesozoic intraplate tectonism of East Asia due to flat subduction of a composite terrane slab. *Earth-Sci. Rev.* 214, 103505.
- Liu, L., Peng, D., Liu, L., Chen, L., Li, S., Wang, Y., Cao, X., Feng, M., 2021a. East Asian lithospheric evolution dictated by multistage Mesozoic flat-slab subduction. *Earth-Sci. Rev.* 217, 103621.
- Liu, L., Stegman, D., 2011. Segmentation of the Farallon slab. *Earth Planet. Sci. Lett.* 311, 1–10.
- Liu, L., Stegman, D.R., 2012. Origin of Columbia River flood basalt controlled by propagating rupture of the Farallon slab. *Nature* 482, 386–389.
- Marquardt, H., Miyagi, L., 2015. Slab stagnation in the shallow lower mantle linked to an increase in mantle viscosity. *Nat. Geosci.* 8, 311–314.
- McQuarrie, N., Wernicke, B., 2005. An animated tectonic reconstruction of southwestern North America since 36 Ma. *Geosphere* 1, 147–172.
- Müller, R.D., Seton, M., Zahirovic, S., Williams, S.E., Matthews, K.J., Wright, N.M., Shepard, G.E., Maloney, K., Barnett-Moore, N., Hosseinpour, M., Bower, D.J., Cannon, J., 2016. Ocean basin evolution and global-scale plate reorganization events since Pangea breakup. *Annu. Rev. Earth Planet. Sci.* 44, 107–138.
- Müller, R.D., Zahirovic, S., Williams, S.E., Cannon, J., Seton, M., Bower, D.J., Tetley, M.G., Heine, C., Breton, E.L., Liu, S., Russell, S.H.J., Yang, T., Leonard, J., Gurnis, M., 2019. A global plate model including lithospheric deformation along major rifts and orogens since the Triassic. *Tectonics* 38, 1884–1907.
- Obayashi, M., Yoshimitsu, J., Nolet, G., Fukao, Y., Shiobara, H., Sugioka, H., Miyamachi, H., Gao, Y., 2013. Finite frequency whole mantle P wave tomography: improvement of subducted slab images. *Geophys. Res. Lett.* 40, 5652–5657.
- Peng, D., Liu, L., Hu, J., Li, S., Liu, Y., 2021a. Formation of East Asian stagnant slabs due to a pressure-driven Cenozoic mantle wind following Mesozoic subduction. *Geophys. Res. Lett.* 48, 1–10.
- Peng, D., Liu, L., Wang, Y., 2021b. A Newly discovered Late-Cretaceous East Asian flat slab explains its unique lithospheric structure and tectonics. *J. Geophys. Res., Solid Earth* 126, e2021JB022103.
- Qi, P., Guo, G., Ren, Y., Cui, M., Wang, X., 2021. Geological characterization of the Eocene Pinghu Movement in the Xihu Sag and its hydrocarbon geological significance. *Geosci.* 35, 1098–1105.
- Rudolph, M.L., Leki, V., Lithgow-Bertelloni, C., 2015. Viscosity jump in Earths mid-mantle. *Science* 350, 1349–1352.
- Schellart, W.P., Freeman, J., Stegman, D.R., Moresi, L., May, D., 2007. Evolution and diversity of subduction zones controlled by slab width. *Nature* 446, 308–311.
- Schmandt, B., Lin, F.C., 2014. P and S wave tomography of the mantle beneath the United States. *Geophys. Res. Lett.* 41, 6342–6349.
- Shen, X., Leng, W., 2021. The mode of trench-parallel subduction of the middle ocean ridge. *Front. Earth Sci.* 9, 781117.
- Si, Q., Xu, C., Gao, S., 2021. Late Mesozoic magmatic arc of East China Sea developed with plate subduction constraints from detrital zircons in well FZ211. *Acta Geol. Sin.* 95, 1743–1753.
- Simpson, R.W., 1997. Quantifying Anderson's fault types. *J. Geophys. Res., Solid Earth* 102, 17909–17919.
- Stotz, I.L., Iaffaldano, G., Davies, D.R., 2018. Pressure-driven Poiseuille flow: a major component of the torque-balance governing Pacific Plate motion. *Geophys. Res. Lett.* 45, 117–125.
- Suo, Y., Li, S., Cao, X., Wang, X., Somerville, I.D., Wang, G., Wang, P., Liu, B., 2020. Mesozoic-Cenozoic basin inversion and geodynamics in East China: a review. *Earth-Sci. Rev.* 210, 103357.
- Suo, Y.H., Li, S.Z., Jin, C., Zhang, Y., Zhou, J., Li, X.Y., Wang, P.C., Liu, Z., Wang, X.Y., Somerville, I.D., 2019. Eastward tectonic migration and transition of the Jurassic–Cretaceous Andean-type continental margin along Southeast China. *Earth-Sci. Rev.* 196, 102884.
- Wei, X.D., Ding, W.W., Christeson, G.L., Li, J.B., Ruan, A.G., Niu, X.W., Zhang, J., Zhang, Y.F., Tan, P.C., Wu, Z.C., Wang, A.X., Ding, H.H., 2021. Mesozoic suture zone in the East China Sea: evidence from wide-angle seismic profiles. *Tectonophysics* 821, 229116.
- Wu, J., Lin, Y.-A., Flament, N., Wu, J.T.-J., Liu, Y., 2022. Northwest Pacific-Izanagi plate tectonics since Cretaceous times from western Pacific mantle structure. *Earth Planet. Sci. Lett.* 583, 117445.
- Yang, C., Li, G., Yang, C.Q., Gong, J.M., Liao, J., 2012. Temporal and spatial distribution of the igneous rocks in the East China Sea Shelf basin and its adjacent regions. *Mar. Geol. Quat. Geol.* 32, 125–133.
- Zhao, Z., Wang, P., Qi, P., Guo, R., 2016. Regional background and tectonic evolution of East China Sea basin. *Earth Sci.* 41, 546–554.
- Zhou, Q., Hu, J., Liu, L., Chaparro, T., Stegman, D.R., Faccenda, M., 2018b. Western US seismic anisotropy revealing complex mantle dynamics. *Earth Planet. Sci. Lett.* 500, 156–167.
- Zhou, Q., Liu, L., Hu, J., 2018a. Origin of Yellowstone volcanic province due to intruding hot mantle driven by ancient Farallon slab. *Nat. Geosci.* 11, 70–76.
- Zhu, W.L., Zhong, K., Fu, X.W., Chen, C.F., Zhang, M.Q., Guo, S.L., 2019. The formation and evolution of the East China Sea Shelf Basin: a new view. *Earth-Sci. Rev.* 190, 89–111.